Synthesis of Shuttle Vehicle Damping Using Substructure Test Results

DANIEL D. KANA* AND STEPHEN HUZAR†
Southwest Research Institute, San Antonio, Texas

An empirical method is developed for predicting the modal damping of a combined parallel-stage Shuttle model by means of damping measurements performed on the individual substructures. Correlations are first determined for each component in terms of damping energy as a function of peak kinetic energy and modal amplitude. The results are then used to predict component damping energies corresponding to the respective kinetic energies and amplitudes that occur for the new modes of the combined System. Modal characteristics for the System, other than damping, are obtained by a real eigenvalue solution of dynamic equations developed by Hurty's procedure of substructures. System equations, which include component modal damping, are also solved by a complex eigenvalue approach for comparison with results of the empirical method. Experimental model components are tested in pin-slip and free-free support conditions, and a combined model is tested in the free-free condition. A variety of damping and mass configurations are included. The empirical method is found to provide damping predictions within 10% to 20% error, while the complex eigenvalue results deviate by as much as 300%, when based only on component modal damping values.

Introduction

Prediction of damping in complex structures is recognized to be extremely difficult because of the presence of various damping mechanisms and the current lack of knowledge in synthesizing even the most elementary mathematical models into combined structural systems. As a result, in initial design procedures in the past, damping characteristics of aerospace systems have usually been predicted at the modal level by empirical methods based on data derived from previous vehicles,[1] and when possible, ultimately verified by actual measurements of modal damping in full-scale dynamic tests. Needless to say, such full-scale testing of large systems is extremely difficult and expensive at best, and has been deemed unfeasible for the Space Shuttle, which will be the largest and most complex aerospace structural system yet attempted.

In order to provide information necessary for predicting dynamic response for Space Shuttle, it is recognized that some new procedure must be developed for this multicomponent system. As a reasonable approach, full-scale testing of the Booster, Orbiter, and any other major components appeared possible, but a requirement would exist for synthesizing this information into a prediction of response for the combined System. Substructuring methods are available,[2] and are presently being further developed[3] for handling prediction of dynamic characteristics of *undamped* structures. However, no accurate method has been derived for including damping in such structural synthesis procedures. Therefore, the purpose of this paper is to present the development of a method which shows a great promise for accomplishing this objective. The philosophy followed in the research program leading to these results has been to perform dynamic tests on individual substructures of a two-component, parallel-stage, rather simple Space Shuttle model, to develop a mathematical model for the components, to combine all of the information into a mathematical model for the combined System, and to compare predicted dynamic characteristics with those obtained from further tests of the combined System.

At the outset of this program it was recognized that enormous efforts have been exerted in the past[4,5] to develop mathematical models of various elementary damping mechanisms, and this work will continue because of the great uncertainty present in the current state of the art in combining these mechanisms in complex structures. It was also recognized that the most reliable methods currently available for measurement of typically light damping in complex structures having reasonable modal separation are those which determine an over-all modal damping at resonance or free decay from resonance conditions. The beauty of the concept of modal damping, of course, is that it results in a single number that represents a reasonable approximation to the aggregate contributions of a multitude of complex damping mechanisms internal to the overall structure. Once it is determined, and some form of relatively simple[6] equivalent mathematical model is matched with the modal values of mass, stiffness, and damping, prediction of dynamic response for that component will be satisfactory at all intermediate frequencies, since damping forces dominate only in the vicinity of resonances. Nonlinearity of damping with amplitude and inevitable relatively wide scatter in damping measurements are two unfortunate dilemmas which must often be faced with this otherwise reasonable approach to the dynamic prediction problem.

In view of the success of modal concepts for synthesis in the past, it appeared reasonable to consider their use for Space Shuttle predictions also, although it is recognized that considerable complications result because of the combination of the substructures into an even more complex System. System natural modes can be expected to occur at frequencies which are intermediate to those for the individual components, and as a result, damping forces which were insignificant in the dynamic response at the intermediate frequencies for the individual structures, now become dominant for the new modes and frequencies. Therefore, the prediction method outlined herein is based on determination of modal damping energy for each component from its own resonance tests, extrapolation of the contribution of each respective component to the total modal damping energy at the new frequencies, and summation of the results for all components. The data presented herein are only typical examples of far more

Presented as Paper 73-400 at AIAA/ASME/SAE 14th Structures, Structural Dynamics, and Materials Conference, Williamsburg, Va., March 20–22, 1973; submitted April 23, 1973; revision received July 30, 1973. Sponsored by NASA Marshall Space Flight Center under Contract NAS8-27569.

Index categories: Structural Dynamic Analysis; LV/M Dynamics, Uncontrolled; Aircraft Vibration.

* Manager, Structural Dynamics and Acoustics. Member AIAA.

† Former Research Engineer.

extensive results which can be obtained from the report[7] from which this paper is condensed.

Description of Physical Model

Configurations

A conceptual drawing of the Space Shuttle model is shown in Fig. 1. It consists basically of Booster and Orbiter model joined together with a pin-joint near the top, and two pin-joints at the end of a rigid link near the bottom. The lower joint simulates a slip-joint for all practical purposes. Each component was made of 2024 aluminum tube of 1-in. o.d. and 0.035-in. wall. Multiple rigid masses were positioned on each to represent the two different mass configurations indicated in Fig. 1. Approximate locations of the masses can be scaled from the figure. These masses were made of split disks of $\frac{1}{2}$-in. thick mild steel and all were nominally 6-in.-diameter and weighed approximately $3\frac{3}{4}$ lb each. Those masses attached to connecting joints included cutouts where necessary to accommodate the joints. These pin-joints were provided through the use of $\frac{1}{4}$-in.-diam., Bendix-Type 5008-600 flexure pivot bearings, that are designed to have extremely low inherent damping.

A list of the notation used for various configurations is given in Table 1, and additional information is given in Fig. 1. It can be seen that two mass configurations were included for several different damping configurations which will be explained momentarily. Both pin-slip and free-free boundary conditions were investigated for the components in order to determine what effect this would have on predictions for the System. (This consideration would also help indicate the type of support structures required for full-scale component testing.) Pin-slip component tests were conducted by mounting the substructure directly to a rigid wall through the upper pin and lower slip-joint. Free-free component tests were conducted by hanging the substructure from a low frequency suspension which was attached to eye-bolts at each side of the second from the top mass (this point was estimated to be a node for most of the lateral bending modes). Finally, System tests were conducted by having the two components attached together with a pin-joint near the top and simulated slip-joint near the bottom, while the entire System was supported on a low frequency suspension attached to a rigid knife-edge nearly under the upper pin-joint. Thus, a simulated over-all free-free suspension was employed.

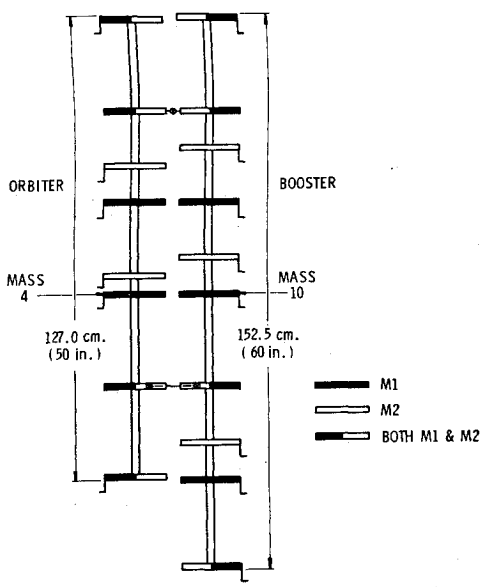

Fig. 1 Conceptual design of space shuttle model.

Table 1 Configuration nomenclature

Vehicle identification
- B = Booster
- O = Orbiter
- S = Combined system

Support
- P = Upper support pinned, lower support slip or double pin.
- F = Components are free-free, system has free-free support but components are joined together as with p-support.

Connecting links
- L0 = No connection.
- L1 = Very low damping (three flexure pins).
- L2 = 0.5% critical damping for system in air first mode.
- L3 = 1.0% critical damping for system in air first mode.
- L4 = 2.0% critical damping for system in air first mode.

Overall structural damping (fluid average viscosities in cp)

	Booster	Orbiter
D0	In air	In air
D1	230	600
D2	1070	1080
D3	4330	4900

Mass distribution
- M1, M2 } See Fig. 1

Damping Mechanisms

It was desirable to use several levels of damping for the over-all structure, as well as provide joint damping in the System. Since repeated tests were contemplated, it was necessary to provide damping in a form that could be controlled as accurately as possible, and be as repeatable and reliable as possible. The actual mechanism whereby damping was provided was arbitrary, so long as it had the above characteristics, and preferably provided damping forces which were linear with amplitude for the sake of increasing measurement reliability. After consideration of several mechanisms for structural damping, a series of wipers acting in oil reservoirs were selected, and the solid structure, including pin-joints was designed to have as low inherent damping as possible.

Angle-shaped wipers were attached to the masses indicated in Fig. 1, and extended into space-fixed individual oil reservoirs. Thus, the model itself was suspended from the laboratory ceiling, and the dampers touched only the oil in its space-fixed reservoirs. Oil viscosity was monitored along with its temperature to allow small corrections to damping values where appropriate. Average values of these viscosities are shown in Table 1. The $D1$ and $D2$ damping was provided by standard motor oils, while the $D3$ damping fluid consisted of a mixture of heavy motor oil and STP oil additive.

Connecting link damping was provided on the Booster side of the lower slip-joint according to the approximate values given in Table 1. Figure 2 shows the mechanism which was found to be most reliable. It consists of a permanent magnet whose flux path is split by a small gap. Part of the magnet is attached to the rigid link while the other part is attached to the connecting rigid mass of the Booster. Relative motion between the two parts of the System is measured by accelerometers A_1 and A_2, whose output is converted to relative velocity and fed back as a voltage into a coil which proportionately modulated the flux path. The low pass filter was necessary to avoid high frequency instabilities in the feedback loop. Although only one such damper was used, similar dampers could have been employed at the other two pin-joints, and the methods to be developed and results obtained would still be valid.

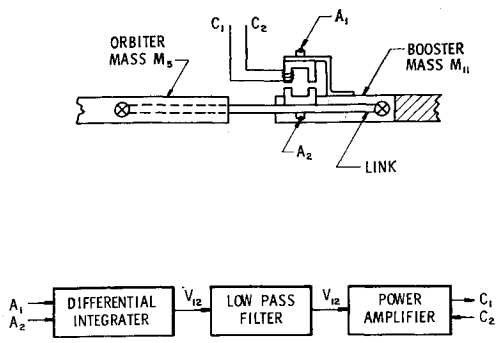

Fig. 2 Link damping mechanism.

Analytical Model

A discrete beam mass analytical model was developed for each the Booster and the Orbiter, and finally they were combined into a System model by means of substructuring techniques. Full details of this model can be obtained from Ref. 7.

Whether one considers an individual component or the combined System, the matrix equation for forced response can be expressed as

$$[\bar{M}]\{\ddot{q}\} + [\bar{C}]\{\dot{q}\} + [\bar{K}]\{q\} = \{\bar{Q}(t)\} \qquad (1)$$

where it is understood that the matrices are generalized with respect to the normal modes of the structure being considered. For the component Booster or Orbiter, $[\bar{M}]$ and $[\bar{K}]$ are diagonalized from the results of a real eigenvalue problem. In this case, the damping matrix $[\bar{C}]$ also can be hypothesized to be diagonal when its elements are based directly on modal damping measurements from component tests. However, when Eq. (1) represents the System, and has been derived by substructuring techniques, the matrix $[\bar{C}]$ is not diagonal when it is similarly based directly on the component modal damping matrices. Further it will be shown later that such a procedure can lead to large errors in damping prediction. Apparently accounting for off-diagonal elements in component matrices is vital in an eigenvalue approach. The method outlined herein avoids this issue.

Experimental Procedures

Background Discussion

In order to utilize damping results from component tests for prediction of System behavior, it was recognized that some form of correlation of component results would first have to be established. Several methods of doing so were investigated. The method finally found to work best is based on a modification of a damping energy correlation which was presented in Ref. 1. However, we now will show that the present modification is necessary in order for the correlation to be valid.

A straightforward dimensional analysis of the component damping results can be performed by considering the following variables: D_c, damping energy dissipated per cycle; M, modal mass; ω, natural frequency of a given mode; x_0, peak modal amplitude for steady-state sinusoidal vibration; and l, some characteristic length. A dimensional analysis results in the nondimensional equation

$$D_c/M\omega^2 x_0^2 = \mathcal{F}_1(x_0/l) \quad \text{or} \quad D_c/T_0 = \mathcal{F}_1(x_0/l)$$

where $T_0 = \frac{1}{2}M\omega^2 x_0^2$ is the peak steady-state kinetic energy at amplitude x_0. This equation can be written in dimensional form as

$$D_c = \mathcal{F}_2(T_0, x_0/l) \qquad (2)$$

This result shows that damping energy is a function of two independent variables, not just kinetic energy alone, as was originally assumed in Ref. 1.

In view of Eq. (2), single-curve correlation will result only if x_0/l is held constant, and a family of curves is obtained, one for each amplitude. Sample results for one Booster configuration are shown in Fig. 3, plotted in the form of Eq. (2). Strictly speaking, the most general procedure for obtaining such data is to measure input energy at each of the component resonances, while holding the amplitude constant. Kinetic energy is computed from measured frequencies and theoretical modal mass. However, for a system with many resonances, it is extremely difficult to obtain accurate measurements at low frequencies, for those amplitudes which are appropriate at higher modes. On the other hand, if the damping forces are found to vary essentially linearly with amplitude x_0, and damping energy linearly with x_0^2, then measurements can be made at any convenient amplitude, and adjusted to the values corresponding to a given value of x_0/l. Further, if this condition does exist, then it is also possible to measure a modal damping ratio ζ by means of conventional free decay or half-bandwidth techniques, and the damping energy can be calculated from $D_c = 4\pi T_0 \zeta$. The latter procedure was utilized in reducing the majority of the data in the present program. However, it should be noted emphatically, that data such as that shown in Fig. 3 can be generated for any form of damping process (including one nonlinear with amplitude), so long as damping energy is measured directly, and amplitudes are either held constant, or values are extrapolated by some suitable procedure.

There is another extremely important point which must be recognized with regard to the form of plot displayed in Fig. 3. That is, the points represent measurements made only at resonant conditions for a given component. When a curve is drawn through these points, we automatically imply that damping energy can be obtained at intermediate, off-resonant kinetic energies as well from these curves. In other words, since we have a system with light damping and reasonably separated modes, Fig. 3 is not only a plot of modal damping energy vs peak modal kinetic energy, but it can be hypothesized to be a plot of total damping energy vs total peak kinetic energy as well, since at resonance, only one mode dominates. The latter statement must hold true regardless of the vibrational form of the component. It would be appropriate to consider measurements at off-resonant conditions to obtain further data to support this assertion, since it will be a fundamental hypothesis to be used in the later development of our method for prediction of System modal damping. However, measurements at such conditions are usually highly inaccurate, and other further evidence which confirms this hypothesis was obtained from other types of measurements.[7]

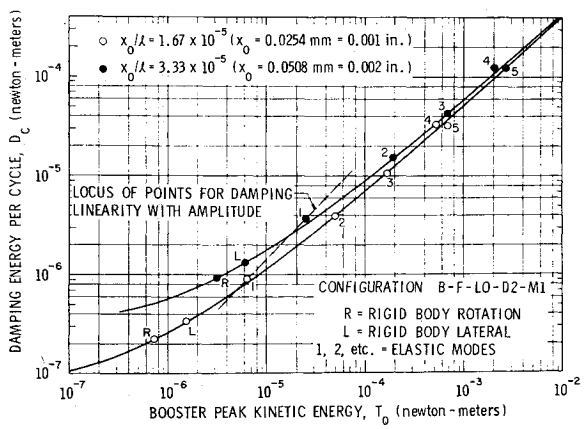

Fig. 3 Influence of peak kinetic energy and amplitude on damping energy for booster model.

General Procedures

It is recognized that the primary emphasis of this program is to develop a method for prediction of System damping. However, in order to do so, use of other dynamic modal properties of the components and the System must be included. Therefore, we will include data to show the effects of a variety of parameters on component behavior, and in many cases will also include predicted values for the components for comparison. These results will establish a confidence in the accuracy of the component mathematical models. We subsequently will then discuss results for the System.

Tests were performed first on each the Booster and Orbiter models for pin-slip and then free-free boundary conditions. Once the apparatus for a given configuration was set up, natural frequencies and mode shapes were measured first. Excitation was provided by a very light electrodynamic exciter which was located at Mass 10 on the Booster and at Mass 4 on the Orbiter (see Fig. 1). For System configurations part of the data were obtained by driving on each component. Mode shapes were measured in the lateral directions only, by means of multiple piezoelectric accelerometers which were mounted to various masses. Most of the accelerometer cables were removed for subsequent damping measurements, since it was found that motion in these cables could cause damping of the same order as the very light structural damping exhibited by the components when tested in air. Damping measurements were performed by the $\frac{1}{2}$-bandwidth technique principally. Careful measures were taken to ensure the reliability of the results. It is estimated that the worst error for modal damping measurements is $\pm 15\%$, although most of the data is much less.

Tests for properties in rigid-body modes were necessary to provide data for System damping prediction. This was a consequence solely of our particular design of providing damping; that is, damping relative to the fixed ground. Axial and lateral tests were conducted by measuring decay rates at the low frequencies (about 1 Hz) of the models on the simulated free-free suspension system. Rotational tests were conducted at about the same frequency by supporting the models on a knife-edge at their c.g. and stabilizing the model with a small lateral spring. In all cases, the same oil levels were maintained as for the tests for elastic modes.

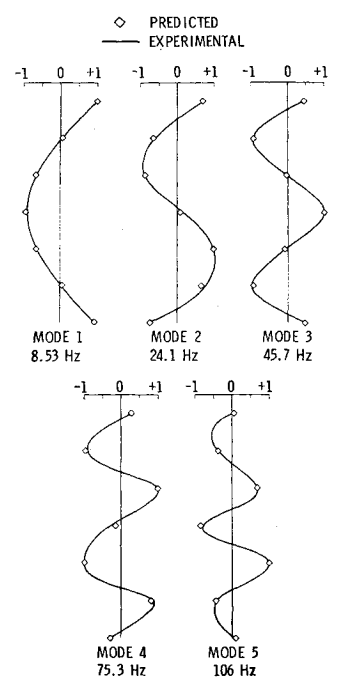

Fig. 4 Booster mode shapes for free-free configurations —$M1$ mass condition.

Link Damper Calibration

The link damping mechanism described in Fig. 2 evolved from a series of other mechanisms which proved to be far more unreliable. It would have been desirable to have calibrated this device with a completely independent apparatus. However, in order to save time, it was decided to calibrate it directly in place on the combined System. It must be emphasized that this in no way deters from the validity of the results that followed. Details of this calibration can be obtained from Ref. 7.

Sample Component Results

Some results for natural modes of the free-free Booster are shown in Fig. 4. The analytical model contained 21 degrees of freedom, and natural frequencies compared within 3% for the indicated modes. Similar results were obtained for the Orbiter, and also both components with pin-slip boundary conditions.

Sample damping results are given for both components with free-free boundaries in Figs. 5 and 5b. In these figures the A, R, and L refer to results for axial, rotational, and lateral rigid body modes, respectively, while the numbers refer to results for elastic modes.

Typical results for component forced responses based on the use of Eq. (1) and measured damping are shown in Figs. 6a and 6b. Similar results were also obtained for other

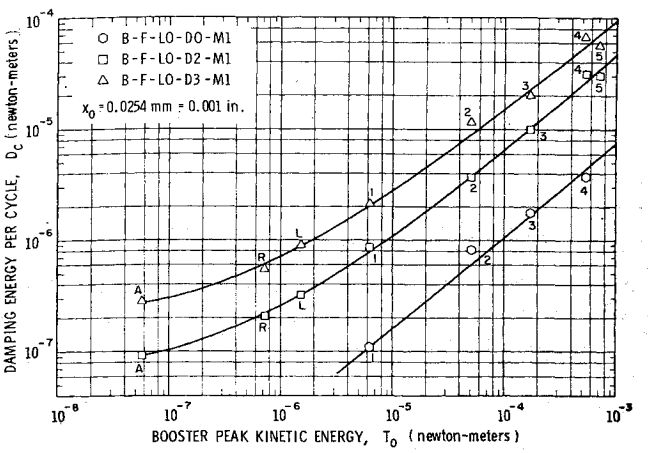

Fig. 5a Experimental damping energy for free-free component configurations—booster.

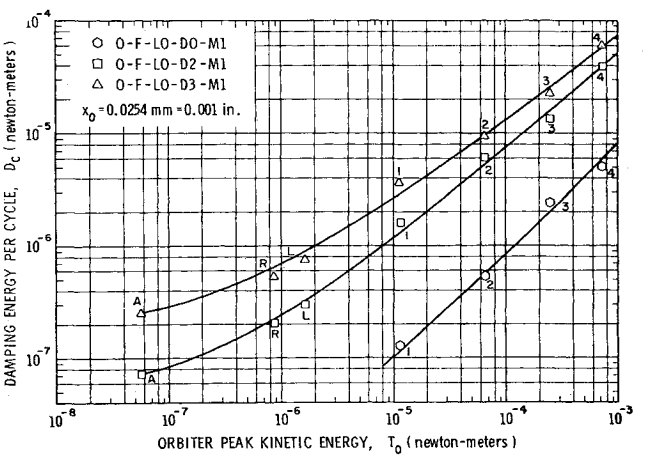

Fig. 5b Experimental damping energy for free-free component configurations—orbiter.

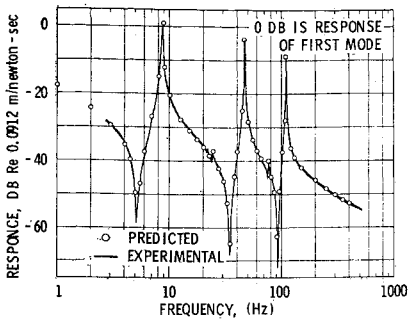

Fig. 6a Booster component response at mass 10 for *B-F-L0-D2-M1* configuration.

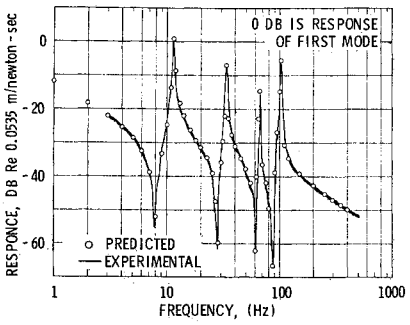

Fig. 6b Orbiter component response at mass 4 for *O-F-L0-D2-M1* configuration.

boundary conditions. Of course, up to this point, nothing presented is significantly new. However, we now consider how these component results will be used to predict combined system results.

Synthesis of System Damping

The comments in Background Discussion, provide the basis for our method of damping synthesis. In particular, we hypothesize that the curves in Figs. 5a and 5b provide a means of selecting an appropriate value of damping energy for each component, once we establish its peak kinetic energy of vibration at a given frequency and amplitude, regardless of the spatial shape it may sustain. In view of this hypothesis, we are now in position to predict the damping values for the combined System. We first perform an ordinary modal analysis of the undamped System. This provides the natural frequencies, mode shapes, and kinetic energies for a given modal amplitude x_0. Let T_{0S}, T_{0B}, and T_{0O} be the kinetic energies for the System, Booster, and Orbiter, respectively, in a given System mode. We note that either the Booster or Orbiter will have an amplitude x_0 while the other component will have some smaller maximum amplitude in that mode. Since the energy curves (Figs. 5a and 5b) are plotted with constant amplitude x_0, the peak displacement of the component having the smaller displacement is scaled so that its peak displacement is now x_0. (This is equivalent to selecting the damping energy from the curve of lower constant amplitude, were such a curve available.) The scale factor is obtained by dividing x_0 by x', where $x' \leq x_0$, and is the maximum amplitude in a given mode on the component having the smaller amplitude. The scale factor may then be written as $S_f = x_0/x' \geq 1$.

For the component having amplitude x_0, we enter the appropriate energy curve and read the damping energy, D_c, corresponding to the kinetic energy $T_0 = \frac{1}{2}M\omega^2 x_0^2$. For the component having an amplitude x', we first multiply the kinetic energy by the scale factor squared so that $T_0 = \frac{1}{2}M\omega^2 x'^2 S_f^2$. We then enter the appropriate energy curve and read a damping energy, D_c'. This damping energy, however, is based on an amplitude x_0. To obtain the actual damping energy we simply divide D_c' by the scale factor squared to obtain actual damping energy, D_c. Once the D_c values are determined for each component, the System damping can then be predicted from

$$\zeta_S = (D_{cB} + D_{cO})/4\pi T_{0S} = D_{cS}/4\pi T_{0S} \qquad (3)$$

The damping ratios obtained using this method are presented later for several system configurations. It should also be pointed out that the above scaling procedure is necessary, since Figs. 5a and 5b indicate that damping energy is a nonlinear function of peak kinetic energy.

Allowance for joint damping is accomplished by adding the damping energy of the joint which is calculated from the calibrated properties of the joint damper and the relative velocity across the joint as given by the theoretical mode shape. The damping ratio for both the link and structure is then obtained by

$$\zeta_{s,l} = (D_{cS} + D_{cl})/4\pi T_{0S} = \zeta_S + \zeta_l \qquad (4)$$

System Results

Natural Modes

System natural frequencies and mode shapes were obtained from synthesis of both the component pin-slip and component free-free modes. For the *M*1 and *M*2 mass configurations the first six pin-slip Booster and first five pin-slip Orbiter modes were used in the synthesis. The first five Booster free-free modes and the first four Orbiter free-free modes were used in the synthesis for the *M*1 mass configuration only. Inspection of *M*1 mass configuration System modes and frequencies showed that the pin-slip component mode synthesis produced much better results at higher frequencies than did the free-free component mode synthesis. Therefore, only the pin-slip component modes were used in the *M*2 mass configuration System synthesis. The System mode shapes obtained from pin-slip component modes and free-free component modes are shown in Fig. 7 for the *M*1 mass con-

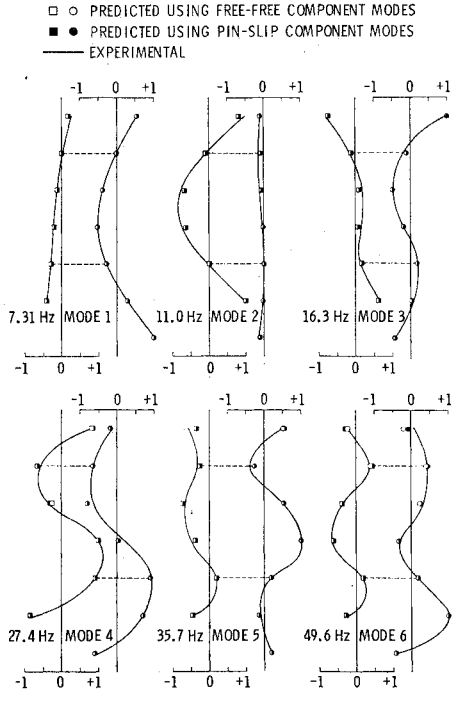

Fig. 7 Combined system mode shapes, *M*1 mass condition.

figuration. Typical results showed that the agreement between the experimental and predicted values is very good to excellent for the pin-slip case up to the tenth mode. Within this range, frequencies agreed within 4%.

Damping

The System damping used to predict System responses was derived from the method outlined in the section, Synthesis of System Damping. In addition to the damping values obtained by our method, we also considered damping values which were obtained from a complex eigenvalue solution of Eq. (1). These values give an indication of the amount of error which could be expected if a straightforward synthesis of damping through the coupling matrices was done. Table 2 gives the System modal damping factors obtained by our method and those obtained from the eigenvalue results. These are presented for the $L1$ link condition only. As pointed out in the section, Sample Component Results, component damping energy was obtained experimentally for both the pin-slip and free-free configurations. Our damping prediction method was applied to both sets of curves, and the results are presented in Table 2.

To obtain the additional modal damping for the various link dampers ($L2$, $L3$, $L4$), we simply add the predicted energy dissipated by the link damper to the predicted energy dissipated by the remaining structure. The predicted link damping energy is given by $D_{cl} = \pi C \Phi_{rel}{}^2 \omega$, where the link damping coefficients C were premeasured, and Φ_{rel} are theoretical mode shape values. Thus, the damping factor for both the structure and link damper is the sum of the individual damping factors as given by Eq. (4). This also provides a further cross check of data by comparing the sum of measured damping factors for the link acting alone and oil acting alone, to measured values obtained when both act simultaneously. Table 3 gives some damping factors for the various structure damping configurations in combination with the $L3$ link damper.

Forced Response

Forced response measurements were made on the Booster at Mass 10 and on the Orbiter at Mass 4 for a constant input force level at Mass 10 in the lateral direction. Figure 8 shows the experimental and predicted forced responses in the form of response in DB vs frequency, similar to the procedures outlined for the component response. Pin-slip, rather than free-free synthesis eigenvectors were used in the expansion of forced response, for it was found that less pin-slip synthesis System eigenvectors are required for sufficient accuracy above the sixth mode.

Conclusions

The results of this study have quite dramatically shown the successful development of a method for predicting damping in combined structural systems with accuracy that is commensurate with that of original measurements made on the substructures, for a relatively simple parallel-stage Shuttle

Table 2 System damping (for $L1$ cases only)

	Mode Number									
S-F-L1-D1-M1	1	2	3	4	5	6	7	8	9	10
Energy prediction[a]	0.0071	0.0089	0.0065	0.0050	0.0049	0.0042	···	···	0.0038	0.0035
Experimental results	0.0070	0.0074	0.0047	0.0046	0.0039	0.0037	···	···	0.0028	0.0032

	Mode Number									
S-F-L1-D2-M1	1	2	3	4	5	6	7	8	9	10
Energy prediction[a]	0.0143	0.0128	0.0103	0.0066	0.0075	0.0066	···	···	0.0057	0.0049
Energy prediction[b]	0.0138	0.0100	0.0088	0.0061	0.0060	0.0053	···	···	0.0046	0.0040
Eigenvalue results	0.0243	0.0135	0.147	0.0277	0.0102	0.0099	0.0082	0.0133	0.0069	0.0103
Experimental results	0.0143	0.0102	0.0079	0.0071	0.0067	0.0053	···	···	0.0043	0.0049

	Mode Number									
S-F-L1-D3-M1	1	2	3	4	5	6	7	8	9	10
Energy prediction[a]	0.0296	0.0237	0.0196	0.0130	0.0133	0.0112	···	···	0.0087	0.0078
Energy prediction[b]	0.0330	0.0226	0.0190	0.0113	0.0120	0.0103	···	···	0.0080	0.0069
Eigenvalue results	0.0562	0.0278	0.0311	0.0607	0.0189	0.0166	0.0133	0.0256	0.0118	0.0193
Experimental results	0.0332	0.0232	0.0172	0.0143	0.0115	0.0105	···	···	0.0080	0.0086

	Mode Number									
S-F-L1-D2/D3-M1	1	2	3	4	5	6	7	8	9	10
Energy prediction[a]	0.0169	0.0238	0.0136	0.0102	0.0088	0.0071	···	···	0.0067	0.0052
Energy prediction[b]	0.0159	0.0208	0.0113	0.0099	0.0074	0.0060	···	···	0.0059	0.0047
Experimental results	0.0169	0.0230	0.0106	0.0106	0.0073	0.0065	···	···	0.0057	0.0054

	Mode Number									
S-F-L1-D2-M2	1	2	3	4	5	6	7	8	9	10
Energy prediction[a]	0.0124	0.0091	0.0080	0.0058	0.0054	0.0053	···	0.0041	0.0044	···
Experimental results	0.0137	0.0106	0.0071	0.0071	0.0050	0.0056	···	0.0067	0.0056	···

[a]Using pin-slip modes.
[b]Using free-free modes.

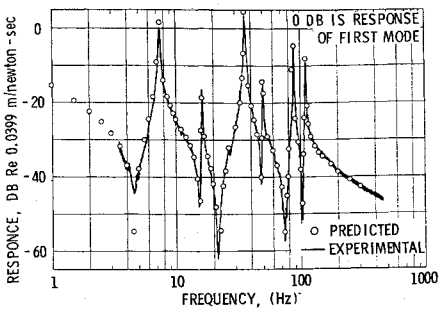

Fig. 8a System response for *S-F-L1-D2-M1* configuration booster—mass 10.

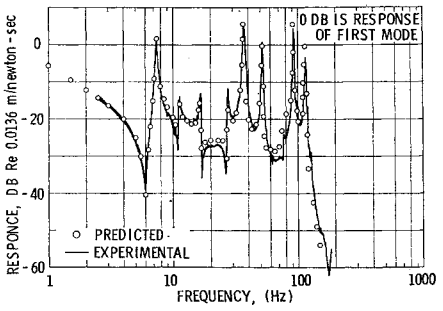

Fig. 8b System response for *S-F-L1-D2-M1* configuration orbiter—mass 4.

model. The application of this method to a more representative model, and for that matter to a prototype, must still be done with caution, and some comments in this regard will be given.

It is first appropriate to discuss the significance of the form of the damping energy results in Figs. 5a and 5b. In essence, each curve represents an aggregate or spatial integration of all of the complex damping processes which occur in the structure. No assumption is made about the particular form of damping present, except that linearity with amplitude was found to be present in these experiments. At the same time, nonlinearity with kinetic energy level exists. It was noted that curves for pin-slip configurations were somewhat different than those for free-free conditions in Figs. 5a and 5b for corresponding mass and damping conditions. In effect, this indicates a significant redistribution of the damping processes for the different boundary conditions. It was determined that this difference results primarily from the presence of longitudinal motion in all pin-slip modes, and the form of damping chosen, which provided higher effective damping for motion in that direction. Of course, this same damping mechanism influenced the free-free modes only through rotational displacements, since the damping reservoirs were located off the longitudinal axis of the models, and only one (rigid-body) orthogonal free-free mode includes longitudinal displacements. At the same time, it appears that the basic component motion (as far as influence damping) in the System modes are more like those of the free-free component modes, rather than the pin-slip modes, since better damping predictions are provided by free-free mode synthesis.

The matter of damping nonlinearity with response amplitude must be mentioned. The concept of plotting damping energy per cycle vs peak kinetic energy is entirely amenable to such a complication. So also is the method of damping prediction developed herein. However, considerable effort will be required in additional testing in order to determine its influence, and it appears that at best, much judgement will have to be exercised to include its effects in any prototype tests.

There is the definite implication that damping energy plots can be used to identify similarities in various different complex structures. In particular, the slopes, shape, curvature, etc., may eventually be catalogued to identify damping processes in many structural applications. Thus, each curve is a plot of some now only empirical damping law, and the identification of parameters with which these laws can be described is a new development.

References

[1] Kiefling, L. and Pack, H., "Structural Damping in Saturn Vehicles and Scale Models," TM X-64607, July 8, 1971, NASA.

[2] Hurty, W. C., "Dynamic Analysis of Structural Systems by Component Mode Synthesis," TR 32-530, Jan. 15, 1964, Jet Propulsion Lab., Pasadena, Calif.

Table 3 System damping (*L3* case only)

	Mode Number									
S-F-L3-D0-M1	1	2	3	4	5	6	7	8	9	10
Energy prediction[a]	0.0112	0.0048	0.0016	0.0015	...	0.0026	...	...	0.0012	...
Experimental results[b]	0.0097	0.0047	0.0019	0.0025	...	0.0017	...	...	0.0010	...
Experimental results[c]	...	...	...	...	...	...	...	...	...	...

	Mode Number									
S-F-L3-D2-M1	1	2	3	4	5	6	7	8	9	10
Energy prediction[a]	0.0250	0.0148	0.0104	0.0076	0.0093	0.0078	...	...	0.0058	...
Experimental results[b]	0.0235	0.0146	0.0119	0.0100	...	0.0076	...	...	0.0040	...
Experimental results[c]	0.0249	0.0161	0.0092	0.0108	...	0.0076	...	...	0.0053	...

	Mode Number									
S-F-L3-D2/D3-M1	1	2	3	4	5	6	7	8	9	10
Energy prediction[a]	0.0271	0.0256	0.0129	0.0114	0.0107	0.0086	...	...	0.0071	...
Experimental results[b]	0.0264	0.0284	0.0108	0.0158	0.0108	0.0064	...	...	0.0057	...
Experimental results[c]	0.0266	0.0277	0.0125	0.0141	0.0131	0.0082	...	...	0.0067	...

[a] Based on component free-free damping energy curves.
[b] Obtained directly from decay records.
[c] Obtained by adding the experimental ζ due to link damping alone to the experimental ζ due to System damping alone.

[3] Forsberg, K. J., "Assessment of Current Methods for Dynamic Analysis of Complex Structures," TM X-52876, Vol. II, July 1970, NASA, pp. 4–27.
[4] Lazan, B. J., *Damping of Materials and Members in Structural Mechanics*, Pergamon Press, New York, 1968.
[5] Snowdon, J. C., *Vibration and Shock in Damped Mechanical Systems*, Wiley, New York, 1968.
[6] Steidel, R. F., Jr., *An Introduction to Mechanical Vibrations*, Wiley, New York, 1971.
[7] Kana, D. D. and Huzar, S., "Synthesis of Shuttle Vehicle Damping Using Substructure Test Results," Interim Report, Contract NAS8-27569, June 1972, Southwest Research Institute, San Antonio, Texas.

DECEMBER 1973 J. SPACECRAFT VOL. 10, NO. 12

Similarity Analysis for the Surface Ablation of Silica-Reinforced Composites

CHIA-LUNG HSIEH* AND J. D. SEADER†
University of Utah, Salt Lake City, Utah

The ablation mechanism of a silica-reinforced composite is approximated as a problem involving a two-phase laminar boundary-layer melt flow with heterogeneous chemical reaction. A model of mixture flow is used to simplify the governing equations, which are converted into a set of ordinary differential equations via similarity transforms. The technique of quasilinearization is utilized to attack this coupled boundary-value problem. It is found that this numerical procedure can converge rapidly to the true solution, if the dimensionless variables and the boundary conditions are properly defined. This is achieved by analyzing the physical nature of the ablation mechanism and the stability and convergence characteristics of the governing equations. The strategy of matching the interface conditions of the molten layer and the gas-boundary layer is also developed, after the solution of the gas boundary-layer flow is analyzed.

Nomenclature

B = dimensionless void fraction $(1-\phi)/(1-\phi_0)$
Cp = specific heat, cal/gm°K
E = activation energy, cal/mole
f = dimensionless stream function
h = specific enthalpy, cal/gm
H_{eff}, H_f, H_p, H_R = heats of ablation, fusion, pyrolysis, reaction, cal/gm
j = volumetric average velocity of the two-phase flow, cm/sec
K = thermal conductivity, cal/sec cm°K
K_e = effective thermal conductivity of the molten layer, cal/sec cm°K
K_R = reaction rate constant, gm/cm² sec
$\dot{m}_a$ = ablation rate, or rate of formation of char, gm/sec cm²
$\dot{m}_l$ = mass transfer rate at the molten layer interface, gm/sec cm²
$\dot{m}_p$ = rate of pyrolysis, gm/sec cm²
$\dot{m}_R$ = rate of carbon-silica reaction, gm/sec cm²
M = ratio of molecular weight of gas-phase to air
n = exponential coefficient of viscosity
p = pressure, atm
Pr = Prandtl number
q = heat transfer rate, cal/cm² sec
q_c = conductive heat transfer rate, cal/cm² sec
q_s = heat transfer rate to the non-ablative surface, cal/cm² sec.
r = body dimension measured normal to the axis of revolution, cm
R = gas constant, 1.987 cal/g-mole °K
R_b = radius of the blunt body, cm
T = temperature, °K
T_r = reference temperature, °K
ΔT = $T_i - T_o$, °K
u = velocity component in the x-direction, cm/sec
u_e = velocity at the edge of the gas boundary-layer, cm/sec/
u_{gj} = drift velocity of the gas-phase in the x-direction, cm/sec
v = velocity component in the y-direction, cm/sec
v_{gj} = drift velocity of the gas-phase in the y-direction, cm/sec
w = mass fraction of the pyrolysis gases
x = coordinate parallel to the body surface, cm
y = coordinate normal to the body surface, cm
β = volume fraction of the liquid phase, $(1-\phi)$
ε = geometric constant
η = dimensionless y-coordinate
θ = dimensionless temperature
μ = viscosity, gm/cm sec
μ_m = apparent viscosity of gas-liquid mixture, gm/cm sec
μ^* = dimensionless apparent viscosity
ρ = density, gm/cm³
$\tilde{s}$ = dimensionless x-coordinate
τ = shear stress, dyne/cm²
ϕ = void fraction of the gas-phase
ψ = stream function, also coefficient of blocking effect

Subscripts

G = gas-phase of the molten layer
i = gas-liquid interface

Received April 19, 1973; revision received August 8, 1973. This study was supported by the AFOSR under Contract F44620-68-C-0022.
Index category: Material Ablation.
* Now Project Engineer, the Amalgamated Sugar Company, Ogden, Utah.
† Professor of Chemical Engineering. Member AIAA.